International Journal of Refractory Metals & Hard Materials 90 (2020) 105232

Contents lists available at ScienceDirect

International Journal of Refractory Metals & Hard Materials

journal homepage: www.elsevier.com/locate/IJRMHM

Characterization of hot-pressed Ti_3SiC_2–SiC composites

Sheida Haji Amiri[a], Mahdi Ghassemi Kakroudi[a,*], Taher Rabizadeh[a], Mehdi Shahedi Asl[b]

[a] Department of Materials Science and Engineering, University of Tabriz, Tabriz, Iran
[b] Department of Mechanical Engineering, University of Mohaghegh Ardabili, Ardabil, Iran

ARTICLE INFO

Keywords:
Ceramic composite
MAX phase
Hot pressing
Characterization

ABSTRACT

The high-density Ti_3SiC_2-SiC composites with different SiC volume contents were fabricated by hot pressing technique under 35 MPa in a vacuum atmosphere at 1550 °C for 30 min. Microstructural observation showed that the distribution of SiC particulates in the Ti_3SiC_2 matrix was uniform which improved the hardness of Ti_3SiC_2–20 vol% SiC sample (13.9 GPa), compared to monolithic Ti_3SiC_2 (7.1 GPa). The sample containing 15 vol% SiC showed the highest flexural strength value, compared to the other Ti_3SiC_2-SiC samples and the monolithic Ti_3SiC_2. The fracture toughness of the Ti_3SiC_2-SiC samples was also lower than that of the monolithic Ti_3SiC_2 MAX phase.

1. Introduction

Ceramics are materials with unique features including high-temperature resistance, high strength, and elastically stiffness, but they suffer from inherent brittleness, low machinability, and thermal shock resistance [1]. Therefore, to tackle these drawbacks, MAX phase ceramics (e.g., Ti_2AlC, Ti_2AlN, Ti_3AlC_2, and Ti_3SiC_2) with a hexagonal structure and combination of properties of both metals and ceramics have recently been produced [2–4]. These materials are a category of ceramics with a main formula of $M_{n+1}AX_n$ where M represents a transition metal, n = 1, 2 or 3, A is an element belongs to IIIA or IVA groups, and X nominates a nitrogen or carbon [5]. Titanium silicon carbide (Ti_3SiC_2) is a MAX phase compound with a layered structure and is an encouraging candidate for high-temperature applications [1–6]. It has hexagonal crystal structure, lattice parameters of c = 1.7669 nm and a = 0.3068 nm [1]. In addition to ease of machinability, this material has excellent properties such as electrical [5,7] and thermal conductivity of 4.5 × 10^6 Ω^{-1} m^{-1} and 40 W/mK, respectively [7], proper thermal shock resistance, high Young's modulus (320 GPa), high toughness (6–11 MPa $m^{1/2}$), moderate flexural strength (260–600 MPa), and low hardness (~4 GPa) [5–8]. Therefore, Ti_3SiC_2 has great potential to be used in high-temperature applications (e.g., heating elements, metal smelting, and automobile engines) and is a suitable substitute for superalloys in many chemical and petrochemical applications [1,8,9].

In recent years, some efforts have been made to develop Ti_3SiC_2-based composite ceramics. In this regard, hard secondary phases (e.g., Al_2O_3 and TiC [1]) have been incorporated into the Ti_3SiC_2 matrix to improve the desired properties. It has been reported that the presence of SiC as a reinforcing phase improves the oxidation [1–5], thermal shock [1], and wear resistance [5–10] of composites. However, a more in-depth understanding of the mechanisms by which a secondary phase performs in a MAX phase matrix is still missing.

Ti_3SiC_2-SiC composites have so far been produced by different methods such as hot-pressing (HP), hot isostatic pressing (HIP), and spark plasma sintering (SPS) [11].

Although many attempts have been made to synthesize Ti_3SiC_2–SiC composites by hot pressing or spark plasma sintering methods, further investigation is required to determine the suitable amount of SiC in which desirable mechanical properties is obtained.

In this research, Ti_3SiC_2-(10–25 vol%) SiC composites were manufactured by hot pressing process. The influences of SiC on the microstructure, physical, and mechanical behavior of the produced composites were investigated by different analytical techniques such as SEM, XRD, and three-point flexural strength tests and compared with the hot-pressed Ti_3SiC_2 monolithic sample.

* Corresponding author.
E-mail address: mg_kakroudi@tabrizu.ac.ir (M. Ghassemi Kakroudi).

https://doi.org/10.1016/j.ijrmhm.2020.105232
Received 2 November 2019; Received in revised form 3 March 2020; Accepted 9 March 2020
Available online 10 March 2020

Table 1
The volumetric percent ratio of Ti_3SiC_2 and SiC used to produce Ti_3SiC_2-SiC composites.

Sample codes	Vol%	
	Ti_3SiC_2	SiC
T	100	–
TS10	90	10
TS15	85	15
TS20	80	20
TS25	75	25

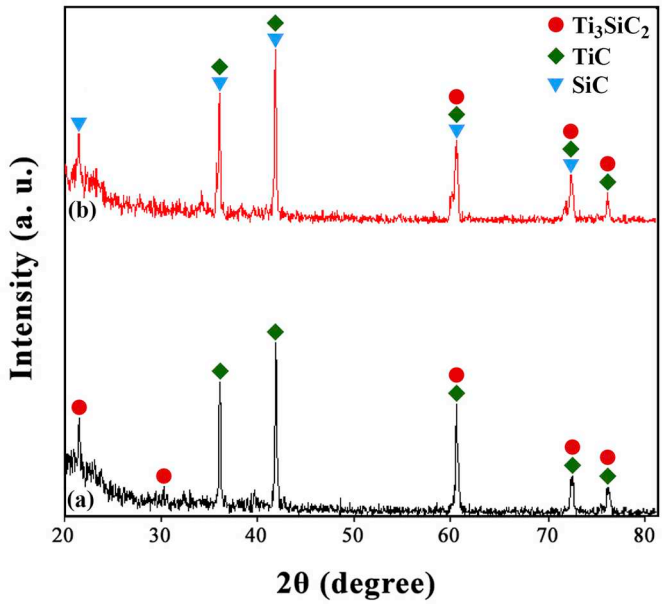

Fig. 1. X-ray diffraction patterns of (a) Ti_3SiC_2 as well as (b) Ti_3SiC_2–20 vol% SiC samples sintered at 1550 °C and 35 MPa for 30 min.

2. Experimental

2.1. Sample preparation

In this research, Ti_3SiC_2 (average particle size: ≤ 15 μm; Xi'AN BIOF BIO-TECH Co. Ltd.) and SiC (average particle size: ≤ 0.7 μm; Xi'AN BIOF BIO-TECH Co. Ltd.) powders were used to fabricate Ti_3SiC_2-SiC composites by hot-press sintering technique. To synthesize Ti_3SiC_2-SiC samples, at first different amounts of Ti_3SiC_2 and SiC powders (in vol%; see Table 1) were mixed in ethanol followed by sonication for 15 min. Afterward, the slurry was wet ball-milled for 70 min with a 250 rpm speed using alumina balls. The ball-to-powder weight ratio was about 1 to 3. The slurry was then dried in the oven at 70 °C for 25 h. For the hot-pressing process, the dried powder mixtures were poured into cylindrical graphite dies with dimensions of 25 × 10 × 10 mm^3. Boron nitride powder with a grain size of about 2 μm and graphite sheets with a thickness of 0.2 mm were used to prevent the adhesion of the mold surfaces to each other, as well as to the produced samples. Finally, thin pieces of graphite sheets with appropriate dimensions were utilized to cover the surfaces in contact with the punch. The hot-pressing process was conducted at 1550 °C for 30 min in a vacuum chamber (5×10^{-2} Pa), and under a pressure of about 35 MPa. At the end of the process, the heating system was turned off, and the furnace was cooled to room temperature. Afterward, the surfaces of the samples were ground by SiC emery paper and then were polished using diamond pastes followed by cleaning ultrasonically in a distilled water bath and dried in air.

2.2. Characterization of the samples

The phase compositions of the initial powders and the hot-pressed specimens were determined by a Bruker D8 X-ray diffractometer. The XRD patterns were analyzed by X'pert high score plus. The surface morphology of the sintered bulks was investigated by a TESCAN field emission scanning electron microscope, equipped with an energy-dispersive X-ray spectroscope.

The density and porosity of the produced specimens were measured by the Archimedes method based on the international standard ASTM C20. To investigate the mechanical characteristics of the prepared composite samples, they were cut into the dimension of 25 × 4 × 3 mm^3 and subjected to a three-point flexural strength test (Zwich/Roell). The three-point flexural strength was calculated considering Eq. 1:

$$S = \frac{PL}{bd^2}\frac{3}{2} \quad (1)$$

where S is the three-point flexural strength in MPa, P is the applied load in N, d is the sample height, and b is the sample width, both in mm and L is the bearing spacing equal to 20 mm. The Vickers micro-hardness of the polished samples was evaluated using a load of 49 N with a soaking time of 16 s (SCTMC HV-1000Z micro-hardness tester). Each micro-hardness value was stated as the average of five measurements.

The fracture toughness of the bulks was estimated by the indentation technique. After Vickers micro-hardness measurement and indentation on the polished surfaces with a load of 49 N for 16 s, the flexural strength was studied with a three-point configuration. In addition, Eq. 2 was used to calculate the fracture toughness of the produced specimens.

$$K_{IC} = 0.016\left[\frac{E}{H_v}\right]^{0.5}\left[\frac{P}{C^{1.5}}\right] \quad (2)$$

where K_{IC} is fracture toughness in MPa√m, E is elastic modulus of porous material in GPa, H_V is Vickers micro-hardness in GPa, P is applied load in N and C is average crack length in μm.

3. Results and discussion

The XRD spectra of monolithic Ti_3SiC_2 and Ti_3SiC_2–20 vol% SiC samples sintered at 1550 °C are shown in Fig. 1. According to Fig. 1 (a), just Ti_3SiC_2 and TiC phases were identified in the XRD pattern of the Ti_3SiC_2 sample, revealing the decomposition of Ti_3SiC_2 during the hot pressing due to the weak carburization resistance of Ti_3SiC_2 (see reaction 1) [12].

$$Ti_3SiC_2 + (3x - 1)C \rightarrow 3TiC_x + SiC \quad (1)$$

In contrast, Ti_3SiC_2, TiC, and SiC phases were observed for the produced Ti_3SiC_2–20 vol% SiC composite, further demonstrating the decomposition of Ti_3SiC_2 as the main constituent of this sample.

To evaluate the microstructure of the produced samples, the

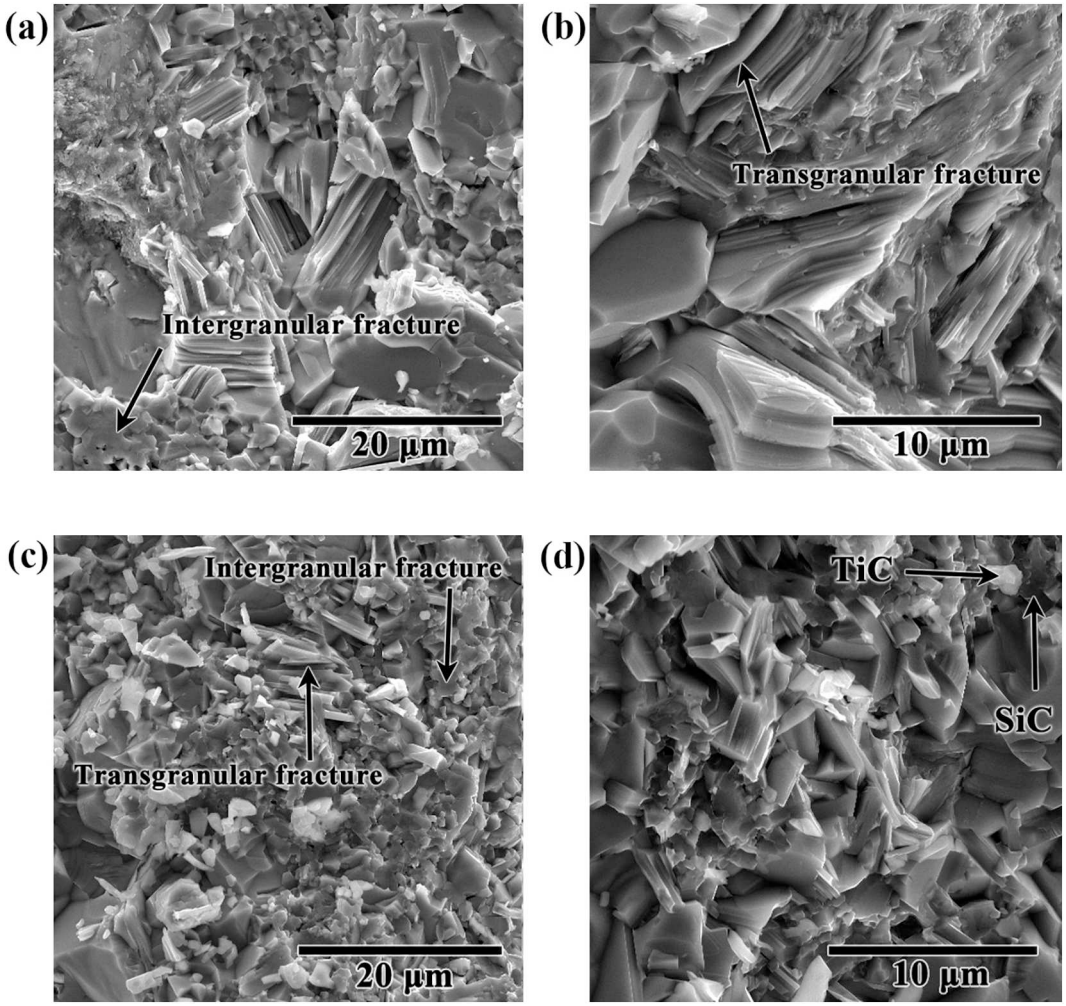

Fig. 2. SEM images of (a,b) Ti_3SiC_2 specimen and (c,d) Ti_3SiC_2–20 vol% SiC composite synthesized at 1550 °C and 35 MPa for 30 min.

fracture surface of the hot-pressed Ti_3SiC_2 specimen and the sintered Ti_3SiC_2–20 vol% SiC composite was studied by SEM and EDS (Fig. 2 and Fig. 3). As can be seen from Figs. 2 (a,b), in the Ti_3SiC_2 specimen, the Ti_3SiC_2 grains with layered morphology were identified. In contrast, the Ti_3SiC_2–20 vol% SiC specimen was composed of layered Ti_3SiC_2 matrix, among which reinforcing SiC (black spots) and TiC (gray spots) particles were uniformly distributed (Fig. 2 c,d). Furthermore, it is worth noting that in both monolithic and composite sample both transgranular and intergranular fracture mode was observed. Such an observation can affect the fracture toughness of the sintered samples, which will be discussed in the last section of this paper. Similar fracture modes were observed in Ti_3SiC_2/Cu/Al/SiC composite reported by Dang et al. [13].

The EDS analysis revealed the presence of Ti, Si, and C peaks in both hot-pressed Ti_3SiC_2 and Ti_3SiC_2–20 vol% SiC samples. For the Ti_3SiC_2 sample, The 1 spot with dark contrast grain indicates the phase combination of SiC, whereas the 2 spot with bright contrast particle points out a TiC phase composition. For Ti_3SiC_2–20 vol% SiC composite, The 1 spot with dark contrast grain Shows the SiC phase, while the 2 spot with gray contrast particle represent the TiC phase. The chemical analysis results are presented in the table next to the diagrams. These results are in good agreement with the XRD patterns of Fig. 1 [14].

Bulk, and relative density together with total, apparent, and closed porosity values of Ti_3SiC_2-X vol% SiC (X = 0, 10, 15, 20, 25) samples are presented in Tables 2. It can be seen from this table that by increasing the volumetric percent of SiC from 0 to 10, the bulk density of the monolithic Ti_3SiC_2 sample decreased from 4.44 g/cm^3 to 4.14 g/cm^3 which was due to the lower theoretical density of SiC (3.21 g/cm^3) compared to Ti_3SiC_2 (4.53 g/cm^3). However, because of the partial decomposition of Ti_3SiC_2 and formation of TiC with a higher theoretical density of 4.91 g/cm^3, the bulk density of samples TS15 and TS20 increased to 4.14 g/cm^3 and 4.20 g/cm^3, respectively. In contrast, the lowest bulk density of 3.83 g/cm^3 was measured for sample TS25 which goes back to (i) a high SiC content in this sample, (ii) the cracks created due to the differences in the thermal expansion coefficients of SiC (5.1×10^{-6}/K [1]) and Ti_3SiC_2 (9.7×10^{-6}/K along c-direction and 8.6×10^{-6}/K along a-direction [1]) as well as (iii) high porosity formation (total porosity: 8.83%; see Table 2). A similar trend was also observed for relative density (see Table 2).

Focusing on the total porosity (Table 2), it can be seen that the total

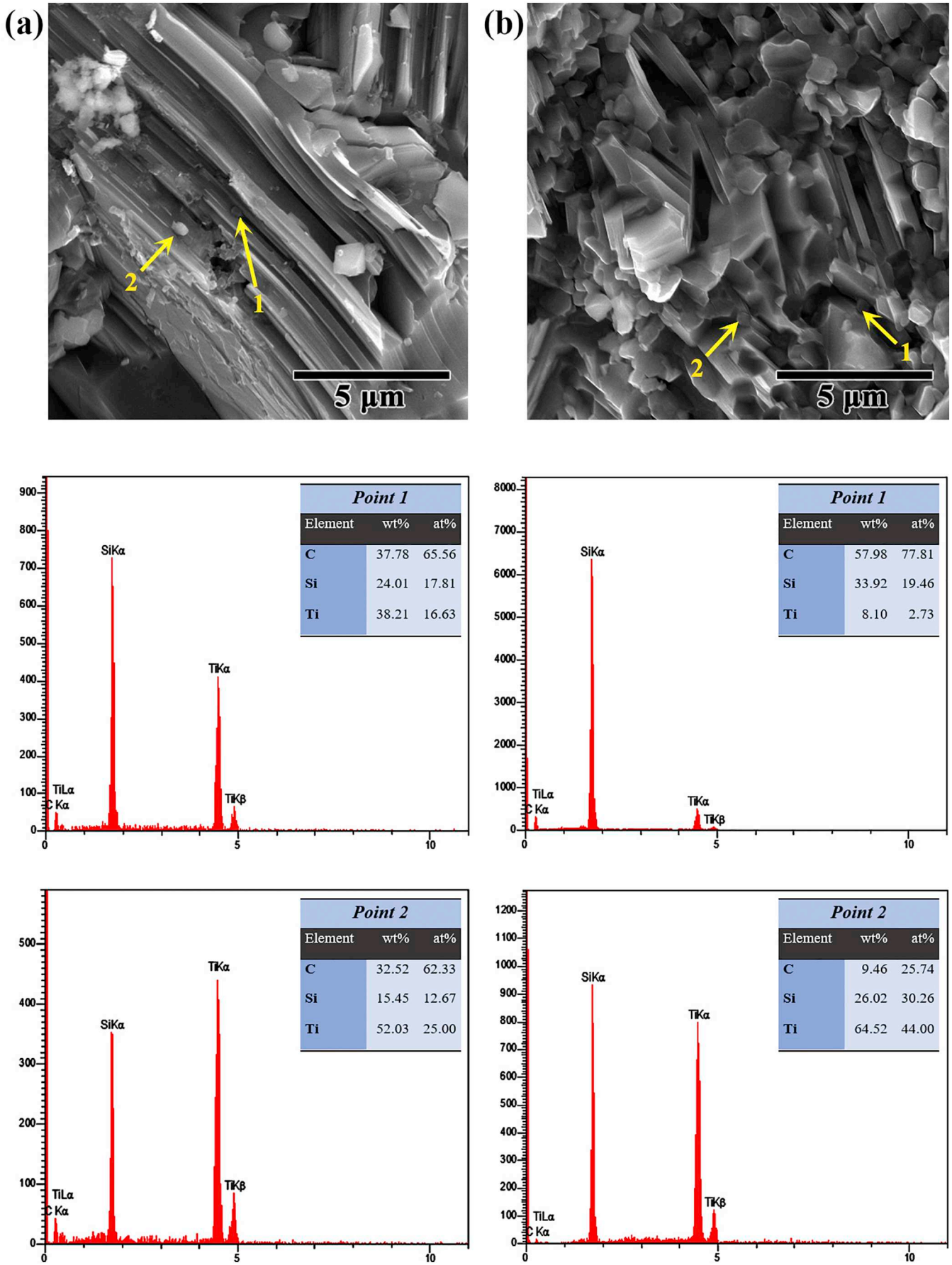

Fig. 3. EDS spectra of (a) Ti_3SiC_2 and (b) Ti_3SiC_2–20 vol% SiC samples sintered at 1550 °C and 35 MPa for 30 min.

Table 2
Bulk, and relative density together with closed, apparent and total porosity values of hot-pressed Ti_3SiC_2-X vol% SiC (X = 0, 10, 15, 20, 25) specimens.

Sample code	Bulk density (g/cm^3)	Relative density (%)	Total porosity (%)	Apparent porosity (%)	Closed porosity (%)
T	4.44	98.08	1.92	1.52	0.41
TS10	4.14	94.14	5.86	2.93	2.93
TS15	4.14	95.60	4.40	4.06	0.33
TS20	4.20	98.48	1.52	2.07	0
TS25	3.83	91.17	8.83	8.26	0.57

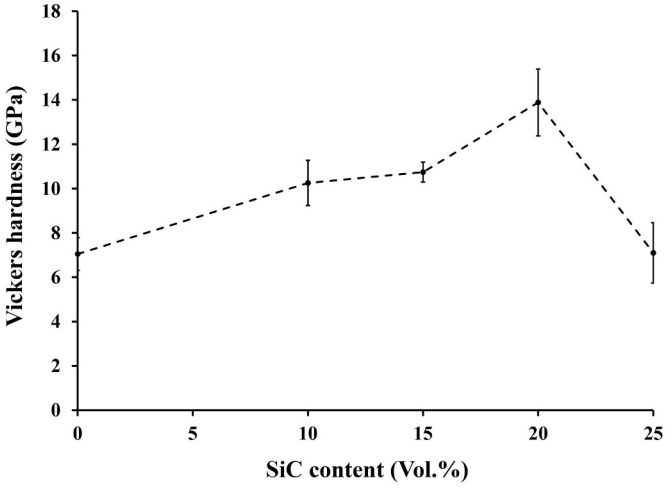

Fig. 4. The Vickers micro-hardness of Ti_3SiC_2-X vol% SiC (X = 0, 10, 15, 20, 25) samples produced at 1550 °C and 35 MPa for 30 min.

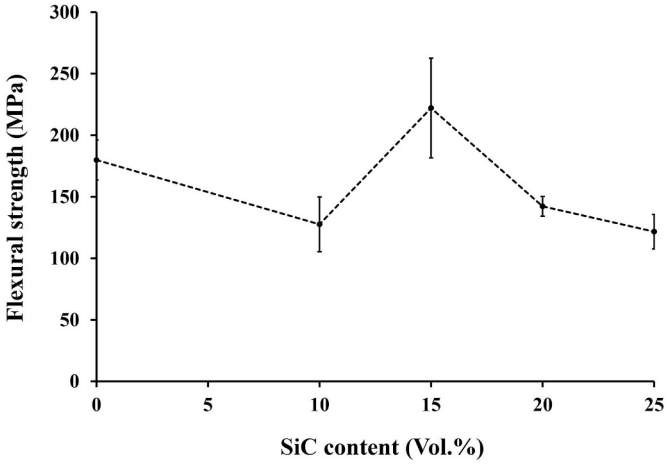

Fig. 5. Flexural strength of hot-pressed Ti_3SiC_2-SiC composites synthesized with different amounts of SiC at 1550 °C and 35 MPa for 30 min.

porosity of the hot-pressed Ti_3SiC_2 sample was 1.92%, of which 1.52% was related to the apparent porosity. However, in sample TS10, the total porosity increased to 5.86%, which was related to the decrease in the relative density of this composite sample (from 98.08% to 94.14%).

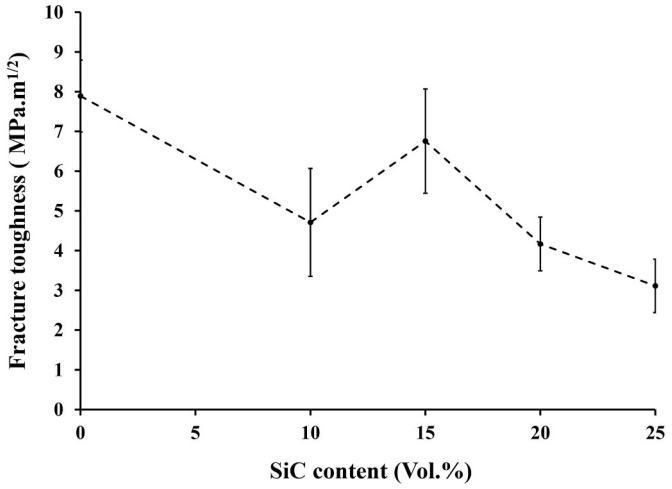

Fig. 6. Fracture toughness of the hot-pressed Ti_3SiC_2-SiC specimens produced without and with different amounts of SiC at 1550 °C and 35 MPa for 30 min.

Moreover, with increasing the relative density in samples TS15 and TS20, the total porosity decreased to 4.40% and 1.52%, respectively. Compared to the other samples, the highest total porosity of 8.83% was measured for sample TS25, and its apparent porosity was higher than the closed porosity (8.26% vs. 0.57%).

The Vickers micro-hardness of Ti_3SiC_2-X vol% SiC (X = 0, 10, 15, 20, 25) specimens was also evaluated, and the obtained results are illustrated in Fig. 4.

As can be observed from Fig. 4, the micro-hardness of the monolithic Ti_3SiC_2 sample was about 7.1 GPa whereas the composite specimens produced with 10, 15 and 20 vol% SiC had higher Vickers micro-hardness values of about 10.3 GPa, 10.7 GPa, and 13.9 GPa, respectively. The poor bonding between the Si atomic layers and the Ti–C–-Ti–C–Ti covalent chain led to the low micro-hardness values of the monolithic Ti_3SiC_2 specimen [15], whilst the presence of hard and reinforcing SiC and TiC particles (HV_{SiC} = 24–28 GPa [10]; HV_{TiC} = 28–35 GPa [16]) increased the micro-hardness of the produced composites. Moreover, in a composite sample, the micro-hardness has a direct relation with grain size [17]. In this research, the addition of SiC decreased the particle size of the hot-pressed samples which caused an increase in the grain boundaries of Ti_3SiC_2-SiC samples, and therefore, the measured micro-hardness (Fig. 2 (c.d) and 4). Furthermore, there is a direct correlation between micro-hardness and relative density. Based on the data presented in Tables 2 and Fig. 4, the relative density of sample TS25 was about 0.075% lower than sample TS20, resulted in about 6.8 GPa lower microhardness of TS25 compared to TS20.

The three-point flexural strength of Ti_3SiC_2-based composites produced with different amounts of SiC was also investigated (Fig. 5). According to this figure, in the absence of SiC, the flexural strength of the hot-pressed specimen was ~179.9 MPa. Whereas, a 0.3% decrease in three-point flexural strength (to 127.6 MPa) was noticed for sample TS10, which was due to the mismatch in thermal expansions of SiC and Ti_3SiC_2. By contrast, because of the partial decomposition of Ti_3SiC_2 and the thermal expansion mismatch between TiC and Ti_3SiC_2 [1], the measured corresponding value for sample TS15 increased to 222.1 MPa. However, when 20 vol% and 25 vol% SiC was used to

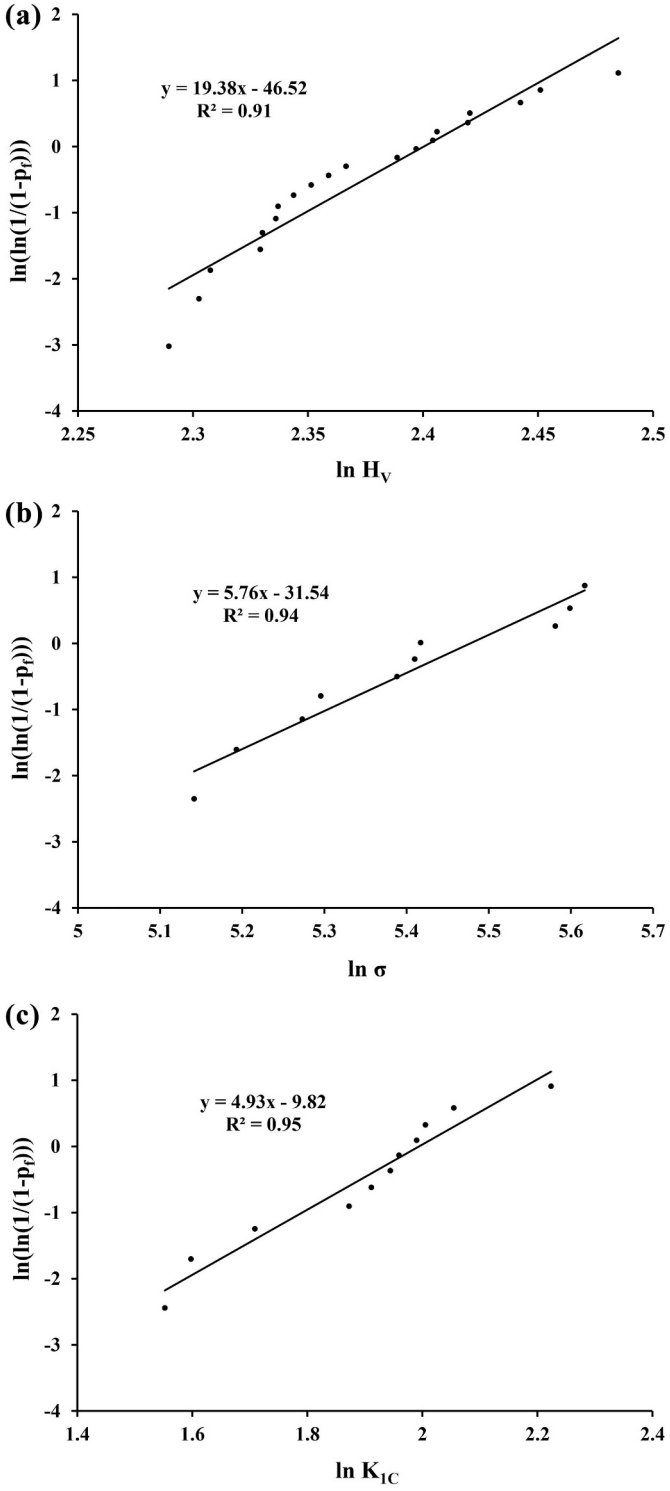

Fig. 7. Weibull plots of the TS15 composite: (a) Vickers hardness, (b) flexural strength, and (c) fracture toughness.

produce samples TS20 and TS25, the flexural strength decreased to 142.2 MPa and 121.6 MPa, respectively, which was probably owing to the presence of SiC agglomerates formed during the sintering process. These findings contradict those of Ghosh [1], who reported lower flexural strength for the Ti_3SiC_2-SiC composites compared to the Ti_3SiC_2 monolithic sample.

Fig. 6, illustrates the variations in the fracture toughness of Ti_3SiC_2-SiC composites prepared in the absence and presence of the different amount of SiC. As shown in this figure, the fracture toughness of the monolithic Ti_3SiC_2 sample was ~8 MPa.$m^{1/2}$. However, a 41% decreased in the fracture toughness (to 4.7 MPa.$m^{1/2}$) was observed for sample TS10, while for sample TS15, the corresponding value increased to 6.8 MPa.$m^{1/2}$. By further increasing the amount of SiC to 20 vol% and 25 vol% SiC, the calculated fracture toughness values decreased to 4.2 MPa.$m^{1/2}$ and 3.1 MPa.$m^{1/2}$, respectively.

The lower fracture toughness of the produced Ti_3SiC_2-SiC composites compared to Ti_3SiC_2 sample could be related to the presence of larger particles in the microstructure of the monolithic specimen which deflected the cracks created during the micro-hardness measurements whilst the decrease in the number of lamellar grains resulted in the straight propagation of the cracks and thus a reduction in the fracture toughness of the composite specimens [17]. Moreover, the fracture toughness of silicon carbide is less than Ti_3SiC_2 (3–5 MPa.$m^{1/2}$ vs. 6–11 MPa.$m^{1/2}$). That means, the cracks may propagate through the particles much more comfortable than the matrix. Furthermore, the hoop stresses around the particles facilitate the crack propagation, and therefore, the loss in fracture toughness [18]. The mismatch in the thermal expansions of the reinforcement/matrix and density are the other parameters affecting the fracture toughness values [19–21]

Compared to the Ti_3SiC_2 monolithic sample, sample TS10 had lower relative density and flexural strength, which resulted in lower fracture toughness. In samples TS15, an increase in both relative density and flexural strength raised the fracture toughness value as well. A similar trend was observed when the amount of SiC increased from 15 vol% to 20 vol% and 25 vol%.

The variability of Vickers hardness, flexural strength, and fracture toughness in the Ti_3SiC_2-SiC composites with different amounts of SiC were analyzed using the Weibull statistical methodology. The Weibull probability plots for the mentioned mechanical properties of TS15 composite are given in Fig. 7. As it can be observed, good linear relationships between ln (ln (1/(1 − p_f))) and ln H_V (Fig. 7a), ln σ (Fig. 7b), and ln K_{1C} (Fig. 7c) are seen, indicating that the experimental results can be well-described with the Weibull distribution formula, where $p_f = i/(n + 1)$, i is the ranking of the property and n is the total of experimented samples. The details of such calculations are explained by Nevarez-Rascon et al. [19]. The statistical properties of the mechanical properties for the different composite samples, applying Weibull method, are summarized in Table 3.

4. Conclusions

Ti_3SiC_2-SiC composites were fabricated by hot pressing from initial powders of Ti_3SiC_2 and SiC. The Ti_3SiC_2-based composites with SiC addition of 10–25% in volume fraction were synthesized to obtain the highest relative density composite. The results show that the highest relative density was related to the Ti_3SiC_2–20 vol% SiC composite because, according to the diffraction pattern of this sample, due to the high temperature of the hot pressing, the TiC phase was formed by the decomposition of Ti_3SiC_2. Addition of SiC as the reinforcing phase improved the mechanical properties such as the Vickers hardness of the Ti_3SiC_2-based composites compared to the monolithic Ti_3SiC_2, and the highest Vickers hardness value related to the Ti_3SiC_2–20 vol% SiC composite with the value of 13.882 GPa. Fracture toughness and

Table 3
Statistical properties of the Vickers hardness, flexural strength, and fracture toughness measured for different composites.

Sample code	Vickers hardness			Flexural strength			Fracture toughness		
	n	Weibull modulus (m)	R^2	n	Weibull modulus (m)	R^2	n	Weibull modulus (m)	R^2
T	20	9.53	0.96	10	10.96	0.94	11	8.46	0.95
TS10	20	9.82	0.96	10	6.25	0.91	11	3.43	0.82
TS15	20	19.38	0.91	10	5.76	0.94	11	4.93	0.95
TS20	20	10.85	0.86	10	17.10	0.99	11	6.18	0.96
TS25	20	6.17	0.89	10	8.44	0.91	11	4.48	0.91

flexural strength of the Ti_3SiC_2-based samples were reduced due to the significant difference in the thermal expansion coefficients of Ti_3SiC_2 and SiC. However, the highest flexural strength was related to the Ti_3SiC_2–15 vol% SiC composite, due to the presence of TiC phases and low difference of thermal expansion coefficient between Ti_3SiC_2 and TiC.

Declaration of Competing Interest

The authors declare that they have no known competing financial interests or personal relationships that could have appeared to influence the work reported in this paper.

References

[1] N.C. GHOSH, Synthesis and Tribological Characterization of in-Situ Spark Plasma Sintered Ti_3SiC_2 and Ti_3SiC_2-TiC Composites, Dhaka, Bangladesh, 2009.
[2] N. Atazadeh, M. Saeedi Heydari, H.R. Baharvandi, N. Ehsani, Reviewing the effects of different additives on the synthesis of the Ti_3SiC_2 MAX phase by mechanical alloying technique, Int. J. Refract. Met. Hard Mater. 61 (2016) 67–78.
[3] O. Dezellus, B. Gardiola, J. Andrieux, S. Lay, Experimental evidence of copper insertion in a crystallographic structure of Ti_3SiC_2 MAX phase, Scr. Mater. 104 (2015) 17–20.
[4] J. Qin, D. He, Phase stability of Ti_3SiC_2 at high pressure and high temperature, Ceram. Int. 39 (2013) 9361–9367.
[5] J. Zhang, T. Wu, L. Wang, W. Jiang, L. Chen, Microstructure and properties of Ti_3SiC_2/SiC nanocomposites fabricated by spark plasma sintering, Compos. Sci. Technol. 68 (2008) 499–505.
[6] M.A. El Saeed, F.A. Deorsola, R.M. Rashad, Optimization of the Ti_3SiC_2 MAX phase synthesis, Int. J. Refract. Met. Hard Mater. 35 (2012) 127–131.
[7] X. Liu, H. Zhang, Y. Jiang, Y. He, Characterization and application of porous Ti_3SiC_2 ceramic prepared through reactive synthesis, Mater. Des. 79 (2015) 94–98.
[8] S.B. Li, J.X. Xie, L.T. Zhang, L.F. Cheng, Mechanical properties and oxidation resistance of Ti_3SiC_2/SiC composite synthesized by in situ displacement reaction of Si and TiC, Mater. Lett. 57 (2003) 3048–3056.
[9] J. Zhang, L. Wang, W. Jiang, L. Chen, High temperature oxidation behavior and mechanism of Ti_3SiC_2–SiC nanocomposites in air, Compos. Sci. Technol. 68 (2008) 1531–1538.
[10] J. Zhang, L. Wang, L. Shi, W. Jiang, L. Chen, Rapid fabrication of Ti_3SiC_2–SiC nanocomposite using the spark plasma sintering-reactive synthesis (SPS-RS) method, Scr. Mater. 56 (2007) 241–244.
[11] S. Li, G.M. Song, Y. Zhou, A dense and fine-grained SiC/$Ti_3Si(Al)C_2$ composite and its high-temperature oxidation behavior, J. Eur. Ceram. Soc. 32 (2012) 3435–3444.
[12] S.B. Li, J.X. Xie, L.T. Zhang, L.F. Cheng, In situ synthesis of Ti_3SiC_2/SiC composite by displacement reaction of Si and TiC, Mater. Sci. Eng. 381 (A) (2004) 51–56.
[13] W. Dang, S. Ren, J. Zhou, Y. Yu, L. Wang, The tribological properties of Ti_3SiC_2/cu/Al/SiC composite at elevated temperatures, Tribol. Int. 104 (2016) 294–302.
[14] H. Abderrazaka, F. Turki, F. Schoenstein, M. Abdellaoui, N. Jouini, Influence of mechanical alloying on Ti_3SiC_2 formation via spark plasma sintering technique from ti/SiC/C powders, Ceram. Int. 39 (2013) 5365–5372.
[15] Y. Zhou, Zh. Sun, Electronic structure and bonding properties in layered ternary carbide Ti_3SiC_2, J. Phys. Condens. Matter 12 (2000) L457–L462.
[16] H.O. Pierson, Handbook of Refractory Carbides and Nitrides, William Andrew Publishing/Noyes, Westwood, 1996.
[17] X. TONG, T. OKANO, T. ISEKI, T. YANO, Synthesis and high temperature mechanical properties of Ti_3SiC_2/SiC composite, J. Mater. Sci. 30 (1995) 3087–3090.
[18] L.H. Ho-Duc, Synthesis and Characterization of the Properties of Ti_3SiC_2/SiC and Ti_3SiC_2/TiC Composites, (2002).
[19] A. Nevarez-Rascon, A. Aguilar-Elguezabal, E. Orrantia, M.H. Bocanegra-Bernal, Compressive strength, hardness and fracture toughness of Al2O3 whiskers reinforced ZTA and ATZ nanocomposites: Weibull analysis, Int. J. Refract. Met. Hard Mater. 29 (2011) 333–340.
[20] M. Akhlaghi, S.A. Tayebifard, E. Salahi, M. Shahedi Asl, G. Schmidt, Self-propagating high-temperature synthesis of Ti_3AlC_2 MAX phase from mechanically-activated Ti/Al/graphite powder mixture, Ceram. Int. 44 (2018) 9671–9678.
[21] M. Akhlaghi, S.A. Tayebifard, E. Salah, M. Shahedi Asl, Ceram. Int. 44 (2018) 21759–21764.